



ELSEVIER

Contents lists available at ScienceDirect

Journal of Marine Systems

journal homepage: www.elsevier.com/locate/jmarsys

Characterization of changes in Western Intermediate Water properties enabled by an innovative geometry-based detection approach

Mélanie Juza^{a,*}, Romain Escudier^b, Manuel Vargas-Yáñez^c, Baptiste Mourre^a, Emma Heslop^d, John Allen^a, Joaquin Tintoré^{a,e}

^a SOCIB, Balearic Islands Coastal Observing and Forecasting System, Palma, Spain

^b CMCC, Bologna, Italy

^c IEO, Malaga, Spain

^d IOC-UNESCO, Paris, France

^e IMEDEA (UIB-CSIC), Esporles, Spain

ARTICLE INFO

Keywords:

Western Intermediate Water
Geometry-based detection
Changes in water mass properties
Glidors and numerical simulation
Western Mediterranean Sea

ABSTRACT

Hydrographic changes in the western Mediterranean Sea (WMED), which is connected to the North Atlantic through the Strait of Gibraltar, may affect the global ocean thermohaline circulation. The Western Intermediate Water (WIW) is a regional water mass which is formed through winter convection processes in the north WMED. The variations of WIW characteristics are hardly detectable by the conventional criterion as defined in the literature and have been poorly addressed. This study introduces an innovative geometry-based method to properly detect WIW. New insights into changes in WIW properties are obtained by applying this method to glider data in the Ibiza Channel and numerical simulation in the whole WMED. Seasonal and interannual variations as well as positive trends in temperature and salinity leading to negative trend in density are highlighted in the Balearic Sea and Gulf of Lion. The basin-scale simulation also shows the spatio-temporal variability of WIW characteristics in the WMED under the influence of the location of formation site, local and regional atmospheric fluctuations, vertical mixing, horizontal advection and mixing with surrounding waters.

1. Introduction

The Mediterranean Sea is considered as a reduced ocean where many ocean processes found throughout the world ocean occur (Malanotte-Rizzoli et al., 2014), making this basin especially interesting for physical, climatic and environmental studies (Bethoux et al., 1999). Environmental factors affect the Mediterranean water masses from the sea surface to the deep ocean and from coastal to open sea waters. These changes affect sea level, as well as marine ecosystems, with a potential associated socio-economic impact. Changes in Mediterranean hydrographic properties could also influence the global thermohaline circulation: the Mediterranean Outflow Water (MOW) interacts with the Atlantic Meridional Overturning Circulation by heat and salt inputs through the Strait of Gibraltar since the salty MOW spreads northwards in the North Atlantic towards the high latitude deep water formation sites (Reid, 1979; Candela, 2001).

The western Mediterranean Sea (WMED) comprises different water masses, originating from the Atlantic Ocean and the Eastern Mediterranean Sea (EMED) or formed in the north WMED (Millot, 1999;

Send et al., 1999; Robinson et al., 2001). In the upper layer, the Atlantic Water (AW) enters the Mediterranean Sea through the Strait of Gibraltar. Circulating through the whole oceanic basin, AW becomes saltier through atmospheric and oceanic processes. Below the surface layer, there is the Levantine Intermediate Water (LIW), which is formed in the EMED (Millot, 1999). Additionally, two water masses are formed in the north WMED through winter convection processes: the Western Intermediate Water (WIW), which is located at intermediate depths, below AW and above LIW (Millot, 1999; Pinot and Ganachaud, 1999), and the Western Mediterranean Deep Water (WMDW) in the deep layer (Millot and Taupier-Letage, 2005; Salat et al., 2010). An additional water mass is the Tyrrhenian Dense Water resulting from the mixing between WMDW and waters of eastern origin (LIW and upper part of the Eastern Mediterranean Deep Water) (Send et al., 1999; Millot et al., 2006).

Temperature and salinity changes in the Mediterranean Sea, and, in particular, warming and salting trends have been detected in the second half of the 20th century (Krahmann and Schott, 1998; Vargas-Yáñez et al., 2010, 2017; Garcia-Martinez et al., 2018). Recent studies agree

* Corresponding author.

E-mail address: mjuza@socib.es (M. Juza).

<https://doi.org/10.1016/j.jmarsys.2018.11.003>

Received 3 July 2018; Received in revised form 11 October 2018; Accepted 20 November 2018

Available online 22 November 2018

0924-7963/ © 2018 The Authors. Published by Elsevier B.V. This is an open access article under the CC BY-NC-ND license (<http://creativecommons.org/licenses/by-nc-nd/4.0/>).

on the increase of both temperature and salinity, especially in the intermediate and deep layers (LIW and WMDW), in the whole WMED (Borghini et al., 2014; Schroeder et al., 2006, 2016) or in sub-basins, such as the Tunisia-Sicily Channel (Ben Ismail et al., 2014; Schroeder et al., 2017), the Ligurian Sea (Marty and Chiavérini, 2010) or the Gulf of Lion (Houpert et al., 2016). Hydrographic changes of WIW have been poorly addressed. WIW is directly impacted by atmospheric conditions and is a sensitive indicator of ocean climate changes. Additionally, the presence of WIW in the Balearic Sea influences eddy formation and the circulation through the Balearic Channels (López-Jurado et al., 1995; Pinot et al., 1995, 2002; Astraldi et al., 1999; Pinot and Ganachaud, 1999; Amores et al., 2013). WIW, which is easily identified by its temperature minimum above LIW, has been traditionally defined according to pre-determined temperature and salinity ranges resulting from regional observational experiments and visual detection (e.g. Salat and Font, 1987; López-Jurado et al., 1995; Vargas-Yáñez et al., 2012). This criterion (hereafter fixed-range criterion) is not adaptive in time and space, and it does not support the detection of interannual changes in hydrographic properties. Alternatively, a visual detection adapting the temperature and salinity ranges can detect such changes but it would be time-consuming and not practical for long time series and spatio-temporal variability studies.

This study proposes an innovative geometry-based criterion to detect and characterize WIW in the WMED. The fixed-range and geometric criteria are compared and evaluated using high resolution data from repeated glider sections in the Ibiza Channel, which is the main pathway of WIW from the northern to the southern WMED (Heslop et al., 2012; Juza et al., 2013), from 2011 to 2017. The detection methods are also applied to the high resolution numerical simulation, called the Western Mediterranean Operational system (WMOP), which covers the WMED, from the Gibraltar Strait to the Sardinia Channel, over the period 2011–2015. The spatially and temporally fully-sampled WMOP outputs are used to extend the analyses of changes in WIW properties to continuous time series in the whole WMED. The new adaptive and automatic criterion enables to detect WIW in case of temporal and regional changes in temperature and salinity properties, to identify the signature of WIW in numerical simulations even when model bias exists (e.g. temperature and/or salinity shift), and to follow the temporal and spatial evolution of WIW characteristics. In this manner, the geometry-based detection method can help to better understand the WIW formation and propagation, its relation with atmospheric and oceanic conditions and thus the ocean processes involved.

This paper is organized as follows. Section 2 provides an overview of the general circulation in the WMED. The fixed-range and geometry-based criteria are described in Section 3. The glider data and numerical simulation are introduced in Section 4. These datasets are then used in Section 5 to evaluate the detection methods. Sections 6 and 7 are dedicated to the analyses of the temporal and spatial variability of the WIW hydrographic properties in the WMED using the geometric criterion. Finally, conclusions and perspectives are given in Section 8.

2. Western Mediterranean Sea overview

The large-scale general surface circulation in the WMED can be characterized by the mean geostrophic velocity derived from the reprocessed interpolated altimetry product (Fig. 1), which is provided by the Copernicus Marine Environment Monitoring Service (<http://www.marine.copernicus.eu>). The Atlantic Jet enters the WMED through the Strait of Gibraltar bringing fresh AW (with salinity around 36.5) at the surface (Viúdez et al., 1996, 1998), which is advected eastwards in the Alboran Sea. AW then reaches the Algerian sub-basin to form the Algerian Current, flowing along the North African continental slope until the Sardinia Channel (Millot, 1999). Circulating in the WMED, AW becomes saltier through air-sea interaction and mixing processes, with salinity values reaching 38–38.3 in the north WMED. A part of AW also joins the EMED where it is partly transformed into Levantine

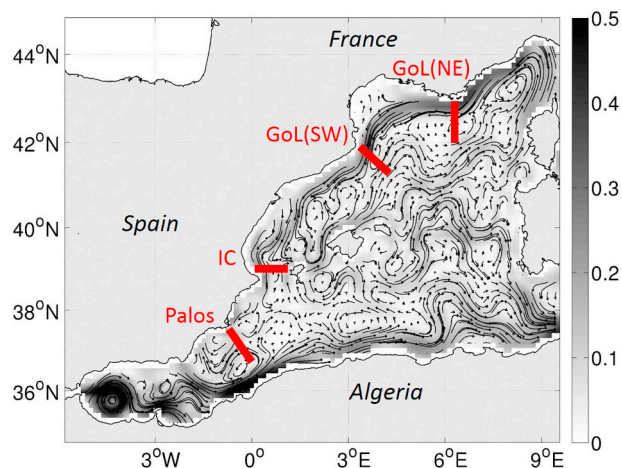


Fig. 1. Mean geostrophic currents (in m/s) from altimetry over the period 2011–2015. The red lines indicate the sections analysed in Sections 6 and 7: north-eastern and south-western Gulf of Lion, Ibiza Channel and Cape Palos (GoL(NE), GoL(SW), IC and Palos, respectively). (For interpretation of the references to color in this figure legend, the reader is referred to the web version of this article.)

Intermediate Water (LIW) by intermediate convection in the Rhodes Island area. LIW enters the WMED through the Sicily Channel and flows out through the Strait of Gibraltar. This water mass is characterized by subsurface temperature and salinity maxima (around 14–13.2 °C and 38.7–38.5 in the WMED, respectively), generally found at 300–400 m depth (Astraldi et al., 1999; Millot, 1999). In the northern WMED, AW and LIW flow northward along each side of Corsica to join and form the Northern Current (NC) in the Ligurian Sea (Millot, 1999). This permanent current flows south-westwards along the French and Spanish coasts reaching the Balearic Sea. Approaching the Ibiza Channel (IC), the NC flows southwards through the western side of the channel reaching the southern WMED; it can also deviate eastwards joining inflows from the southern basin that can cross the Balearic channels to form the Balearic Current along the northern continental slope of the Balearic Islands (Pinot et al., 1995, 2002; Heslop et al., 2012).

In the north WMED, WIW is formed by intense water cooling and vertical downward mixing of AW. Despite the influence of low salinities of continental origin, the continental shelves in the Gulf of Lion (GoL) and the Ebro delta region in the Balearic Sea are the main places of WIW formation (Millot, 1999; Pinot and Ganachaud, 1999; Salat et al., 2010; Juza et al., 2013). This water mass is also formed around deep convection areas from the Ligurian Sea to the Balearic Sea (Millot, 1999). GoL is also the place where WMDW is formed through deep convection (Salat et al., 2010).

3. Detection methods

3.1. Fixed-range criterion

The conventional fixed-range criterion to detect WIW is based on potential temperature (θ) and salinity (S) ranges according to fixed values which were determined from regional oceanographic campaigns:

- $\theta < 13$ °C, $38.1 < S < 38.3$ (Salat and Font, 1987)
- $\theta < 13$ °C, $37.7 < S < 38.3$ (López-Jurado et al., 1995)
- $11.5 < \theta < 13$ °C, $37.7 < S < 38.3$ (Vargas-Yáñez et al., 2012)

In this study, the fixed-range criterion values refer to López-Jurado et al. (1995) which is used in previous studies in the north WMED (e.g. Heslop et al., 2012; Juza et al., 2013).

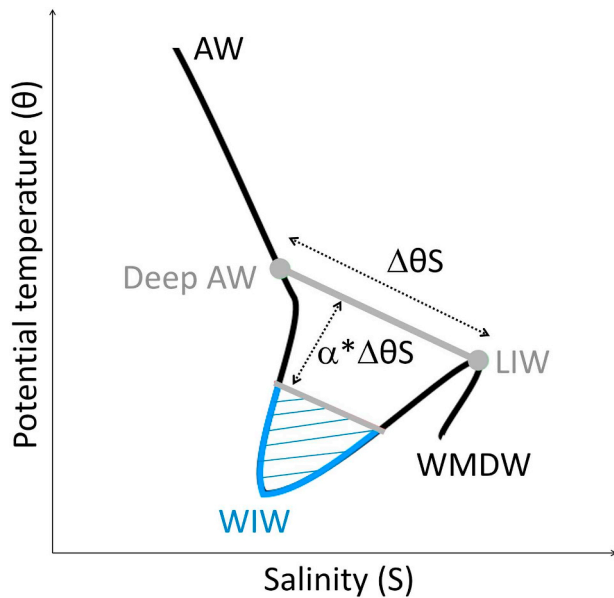


Fig. 2. Schematic θ/S diagram with the typical water masses of the WMED (AW, WIW, LIW, and WMDW) and WIW geometry-based detection procedure (described in Section 3).

3.2. Geometry-based criterion

The geometric method is based on the WIW definition and the θ/S diagram shape. Indeed, WIW is a mode water, characterized by its nearly vertical homogeneity caused by vertical convection, with a θ absolute minimum. This method is inspired by the way that oceanographers visually define WIW on a θ/S diagram.

The general principle of this approach is to detect WIW from LIW in a θ/S diagram (Fig. 2). Indeed, LIW is relatively easy to detect (maximum of S and local maximum of θ) and WIW is a water that presents a sharp curvature of the θ/S profile above LIW. Therefore, after determining the LIW position on the θ/S diagram, the deep AW is identified by applying a density difference ($\Delta\rho$) to the LIW density to obtain the density value of deep AW. WIW is then detected as the θ/S points that are significantly colder than the line between these two waters on the θ/S diagram (this line represents normal mixing). The detailed geometry-based method is as follows:

- **Determination of the density (ρ) value of LIW.** First, the LIW S maxima are found considering the points between the 95 and 99th percentiles of S to avoid picking up spurious values and above a selected depth (lim_depth) to discard deep water values. Then, the ρ value of LIW is given by the point where θ is maximum within this selection.
- **Determination of the ρ value of deep AW.** The deep AW ρ is given by the LIW ρ minus $\Delta\rho$. When no such ρ is found in the profile, the surface value is considered if it is not too close to the LIW value (higher than $0.7 * \Delta\rho$). The identified deep AW corresponds to cold and dense AW that might be convected and form WIW. Only profile points between LIW and deep AW (grey points in Fig. 2) are now considered.
- **Computation of the line between LIW and deep AW.** For each profile, the line ($\Delta\theta S$) on the θ/S diagram (Fig. 2) is computed.
- **The threshold distance to the ($\Delta\theta S$) line** to characterize WIW is determined as follows: the distance between LIW and deep AW is computed $\Delta\theta S = (\sqrt{\Delta\theta^2 + \Delta S^2})$ and multiplied by the coefficient α .
- **Identification of WIW.** WIW corresponds to the points whose distance to the line is greater than the threshold distance, which is similar to find θ minimum.
- **Extrapolation in formation area:** WIW can also be detected on the

coast (where there is no LIW) when recently formed in this area, considering profiles with θ/S values close to the previously identified WIW characteristics. The extrapolated WIW θ/S points are determined as follows: θ maximum is the 80th percentile of the previously detected WIW θ , S is within the WIW S range extended to $\pm \Delta\text{lim}S$, and depth is above lim_depth .

- **The parameters for the WIW in the WMED** have been defined as follow:

$$\text{lim_depth} = 500 \text{ m}; \Delta\rho = 0.32 \text{ kg/m}^3; \alpha = 0.14; \Delta\text{lim}S = 0.03.$$

The parameter lim_depth has been introduced to insure that the deep waters are not considered in the determination of LIW. Hence, its value has been fixed below the LIW core, which is generally found at 300–400 m in the WMED (Millot, 1999; Garcia-Martinez et al., 2018). Moreover, $\Delta\rho$ has been fixed according to the typical water mass θ/S values of the WMED. In particular, it has been inspired by the climatological values of AW and LIW as found from the glider data used in this study (described in Section 4.1) and in Garcia-Martinez et al. (2018) in the WMED. Contrary to the latter parameters which are fixed values, the parameter α may need to be tuned. Due to more homogeneous θ in the intermediate layer in the WMOP simulation than in observations, the coefficient α is adjusted and fixed to 0.08 for the model. Finally, the geometry-based detection method is applied to an ensemble of vertical hydrographic profiles from gliders and model data since distribution properties are used in the detection procedure.

The geometric criterion is time evolutive adapting to changes in water mass characteristics. It can be applied to long-time series at regional scale in order to address the variability at the spatial and temporal resolution of the θ/S diagrams.

4. Datasets

4.1. Glider data

Gliders, operated by the Balearic Islands Coastal Observing and Forecasting System (SOCIB), are deployed in the IC following a semi-continuous endurance line (Heslop et al., 2012; Tintoré et al., 2013) since January 2011. The transect line corresponds to the section at 39°N in Fig. 1. Every mission corresponds to the deployment of one glider which monitors several transects in the IC, one crossing lasting approximately 3–4 days. For technical and operational reasons, the mission duration and the temporal coverage remain uneven (Table 1). Slocum deep gliders provide high-resolution in situ hydrographic data until 1000 m depth with a horizontal resolution of around 2 km when profiling to full depth. The gliders were fitted with SeaBird CTD sensors. Taking into account the instrument accuracy and stability in conductivity and temperature, as well as the calibration frequency, the salinity accuracy is estimated around ± 0.01 . This instrument calibration error has no impact on the results presented in this study. The glider repeated sections allow to characterize accurately the water mass properties from daily-weekly to interannual time scales in the IC. In this study, 40 glider missions from 2011 to 2017 are considered using the L2 glider product (Troupin et al., 2015): θ and S data are interpolated on a regular vertical grid with 1 m vertical resolution which corresponds approximately to the glider sampling. The spatial positions of the θ/S profiles vary with time.

4.2. Numerical simulation

The high resolution Western Mediterranean Operational system (WMOP, Juza et al., 2016) is based on a regional configuration of the Regional Ocean Modelling System (ROMS; Shchepetkin and McWilliams, 2003, 2005) in the WMED (Fig. 1) from Gibraltar Strait (6°W) to Sardinia/Corsica islands (9.2°E). The vertical grid is made of 32 terrain following sigma levels stretched at the surface and the bottom. The horizontal resolution is $\sim 1/50^\circ$ (~ 2 km). The bathymetry

Table 1

WIW detection using the fixed-range and geometric methods for gliders and interpolated model in the IC from 2011 to 2017. Yes (no) notifies the presence (absence) of detected WIW. Detection types (similar, more, new) are described in Section 5.1.

Glider missions (starting month)	Duration (in days)	Fixed-range/geometry criterion in gliders	Fixed-range/geometry criterion in WMOP
Jan 2011	19	Yes/yes (more)	No/Yes (New)
Feb 2011	18	Yes/yes (similar)	No/yes (new)
Mar 2011	15	Yes/yes (similar)	Yes/yes (more)
May-Jun 2011	13–13	Yes/yes (more)	Yes/yes (more)
Mar 2012	13	Yes/yes (more)	No/yes (new)
May 2012	15	Yes/yes (more)	No/no
Jul-Aug 2012	15–16	No/yes (new)	No/no
Oct-Nov 2012	4–7	No/no	No/no
Jan 2013	14	No/no	No/no
Mar 2013	14	Yes/yes (more)	Yes/yes (more)
May-Jul 2013	13–16	Yes/yes (more)	No/yes (new)
Sep 2013	15	Yes/yes (more)	No/no
Nov-Dec 2013	3–14	No/no	No/no
Feb-Apr-Jul 2014	15-23-16	No/no	No/no
Oct-Nov 2014	16–16	No/no	No/no
Jan-Mar-Apr 2015	25-8-27	No/yes (new)	No/yes (new)
Jun-Aug-Oct 2015	17-16-17	No/no	No/no
Sub-total	29 missions	2 “similar detection” 9 “more detection” 5 “new detection”	0 “similar detection” 4 “more detection” 8 “new detection”
Jan-Feb-Apr-Jul 2016	15-43-46-25	No/yes (new)	Not available
Sep 2016	22	No/no	Not available
Oct-Dec 2016	26–40	No/yes (new)	Not available
Mar-Jul-Sep 2017	38-17-28	No/yes (new)	Not available
Nov 2017	20	No/no	Not available
Sub-total	11 missions	9 “new detection”	–
Total	40 glider missions 29 model missions	2 “similar detection” 9 “more detection” 14 “new detection”	0 “similar detection” 4 “more detection” 8 “new detection”

is derived from a 30" database (Smith and Sandwell, 1997) corresponding to a resolution around 1.5 km in the Mediterranean. The simulation is initialized and nested in the daily larger scale 1/16° CMEMS MED-MFC model (Simoncelli et al., 2014). The high resolution HIRLAM atmospheric fields (Undén et al., 2002; 3 h, 1/20") provided by the Spanish Meteorological Agency (AEMET) are used to compute surface turbulent and momentum fluxes through bulk formulae (Fairall et al., 2003). Runoffs of the six major rivers of the modelling domain (Var, Rhône, Aude, Hérault, Ebro and Júcar), which are provided by the French HYDRO database (<http://www.hydro.eaufrance.fr>) and the Spanish hydrographic confederations of Ebro and Júcar rivers (<http://www.chebro.es>; <http://www.chj.es>), are specified as point sources of low saline water. Daily values of observed river discharge are used. An explicit momentum diffusion is applied, since it was found to improve the representation of mesoscale activity, particularly in the Algerian basin. This free run hindcast simulation is performed over the period 2009–2015. Elements of validation of this simulation can be found in Moure et al. (2018).

4.3. Data processing

The glider data are analysed over the period 2011–2017. The outputs of the simulation are linearly interpolated at the observations space-time positions for their assessment and comparison with glider data over their common period 2011–2015. Then, the fully-sampled simulation is used to follow the spatio-temporal evolution of the WIW properties, using the continuous time series and extending the analyses

to adjacent sub-regions. More precisely, WIW characteristics will be analysed along four specific sections (displayed in Fig. 1). In the north-eastern sub-basin, the meridional section at 6.3°E (GoL(NE) in Fig. 1) crosses the NC west of the Ligurian Sea where WIW may be formed and east of GoL which is the main area of WIW formation. Further downstream along the NC in the south-western GoL is the second section of the study between 3.3 and 4.2°E (GoL(SW) in Fig. 1). Further south, in the Balearic Sea, the section at 39°N, from 0.1 to 1.1°E, corresponds to the endurance line monitored by the glider in the IC. Approaching the Alboran Sea in the southern sub-basin, the WIW presence will be also analysed at Cape Palos.

5. Evaluation of detection methods

5.1. Comparisons along glider tracks

The fixed-range and geometry-based WIW detection methods are compared using the glider and interpolated simulation data for every glider mission in the IC over 2011–2015. The method evaluation is extended to 2017 with glider data given their availability in more recent years. The results for the 40 missions are shown in Table 1. Three types of results are identified: similar detection, i.e. similar points identified as WIW, with both methods (hereafter “similar detection”), detection in both methods with more WIW θ/S values caught by the geometric method than with the fixed-range criterion (hereafter “more detection”), and detection only with (and thanks to) the geometric method (hereafter “new detection”). Note that there is no case of less detection with the geometry-based method meaning that all previously detected WIW will be detected with the new method. These three situations are illustrated in Figs. 3 and 4 depicting θ/S diagrams.

For 38% (59%) of the missions in glider (model) data, which were mostly deployed in summer-fall and during the year 2014, no WIW is detected with both methods in both datasets (Table 1). Similar WIW detection with both methods occurs for only two missions in February and March 2011 in the glider data (Fig. 3a). For the other missions, mainly deployed in winter-spring, more WIW θ/S values are detected in glider and model data with the geometric method while no or fewer WIW is detected with the fixed-range criterion. More precisely, observed WIW is detected with both criteria in winter-spring 2011 and 2012, but more WIW θ/S values are caught by the geometric criterion (as illustrated in Fig. 3b). The additional detected volume is warmer than 13 °C in 2011 and 2012, and saltier than 38.3 in 2012 (i.e. exceeding the θ and S limits of the fixed-range criterion). In spring-summer 2013, WIW also covers a wider range of S including values saltier than 38.3. The new criterion enables to detect a larger volume with saltier WIW. It also allows to catch the few WIW which is present in summer 2012. In winters 2015–2016–2017, WIW is warmer and can be detected only by the geometric criterion (as displayed in Fig. 3c). The new method enables to capture WIW changes, in particular when WIW becomes warmer than 13 °C as since 2015. In the simulation, WIW is not (or partially) detected in 2011, 2012 and 2013 with the fixed-range criterion due to the model S shift with values saltier than 38.3. However, WIW is present in WMOP, as revealed by the distinct θ minima in the θ/S diagrams (as illustrated in Fig. 4). Thanks to the geometric criterion, simulated WIW is caught where it was detected in observations (Fig. 4a, b). In winter 2015, despite the model bias towards higher θ and S values, the geometric criterion allows to automatically detect WIW warmer than 13 °C as in the observations (Fig. 4c).

The θ/S diagrams have been subject to visual inspection and evaluated independently by oceanographers for all glider missions. The new criterion, which is based on the well-marked curvature of WIW in the θ/S diagram, detects more WIW which is distinctly present. Moreover, oxygen (O₂) concentration data, which were partially collected during the glider missions in the IC, have shown that the detected WIW points have temperature minima coinciding with high O₂ concentration

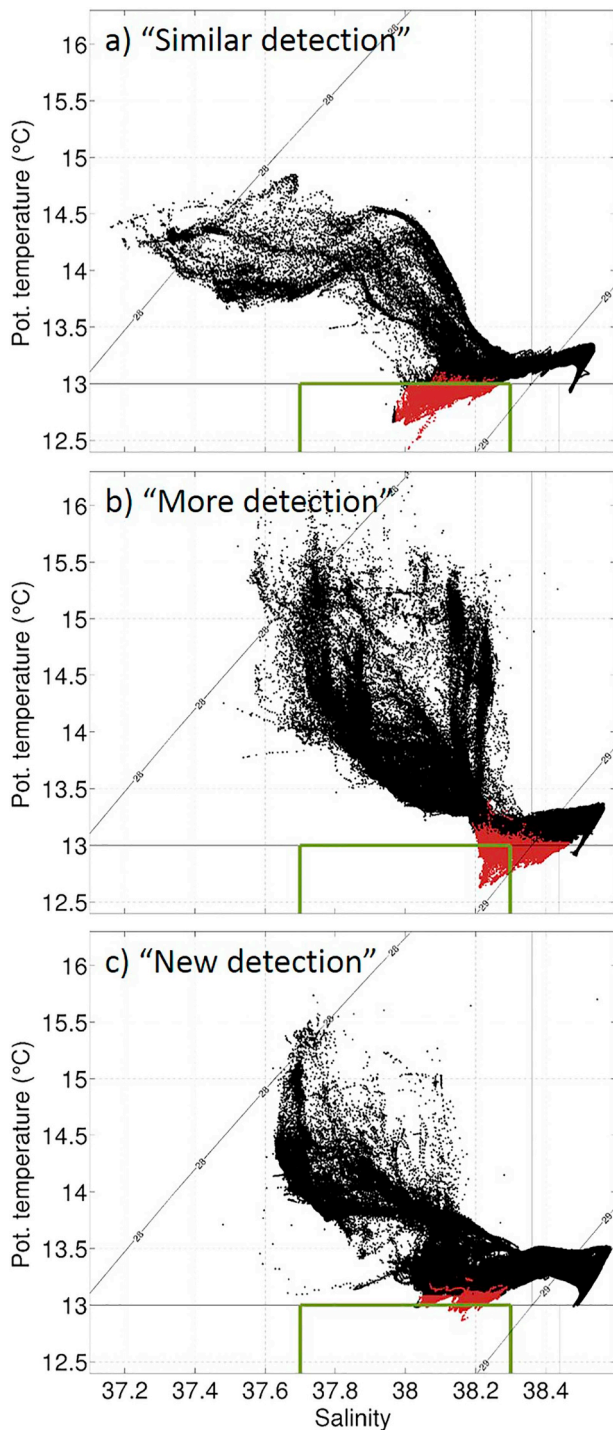


Fig. 3. θ/S diagrams from glider during the missions in February 2011 (a), March 2012 (b) and March 2015 (c). The green box delimits the fixed-range criterion values for WIW. The red points correspond to WIW detected by the geometric method. The missions a), b) and c) illustrate the three types of detection results found in glider data. (For interpretation of the references to color in this figure legend, the reader is referred to the web version of this article.)

values (i.e. ventilated waters) in the range of 210–250 $\mu\text{mol/L}$ (not shown). These preliminary results also seem to confirm the reliability of the geometric method. We can therefore state that this new method is more accurate than the fixed-range criterion, and enables to capture WIW in the IC in case of changes in properties (e.g. warming and/or salting as it occurs especially in recent years) and/or θ/S model errors.

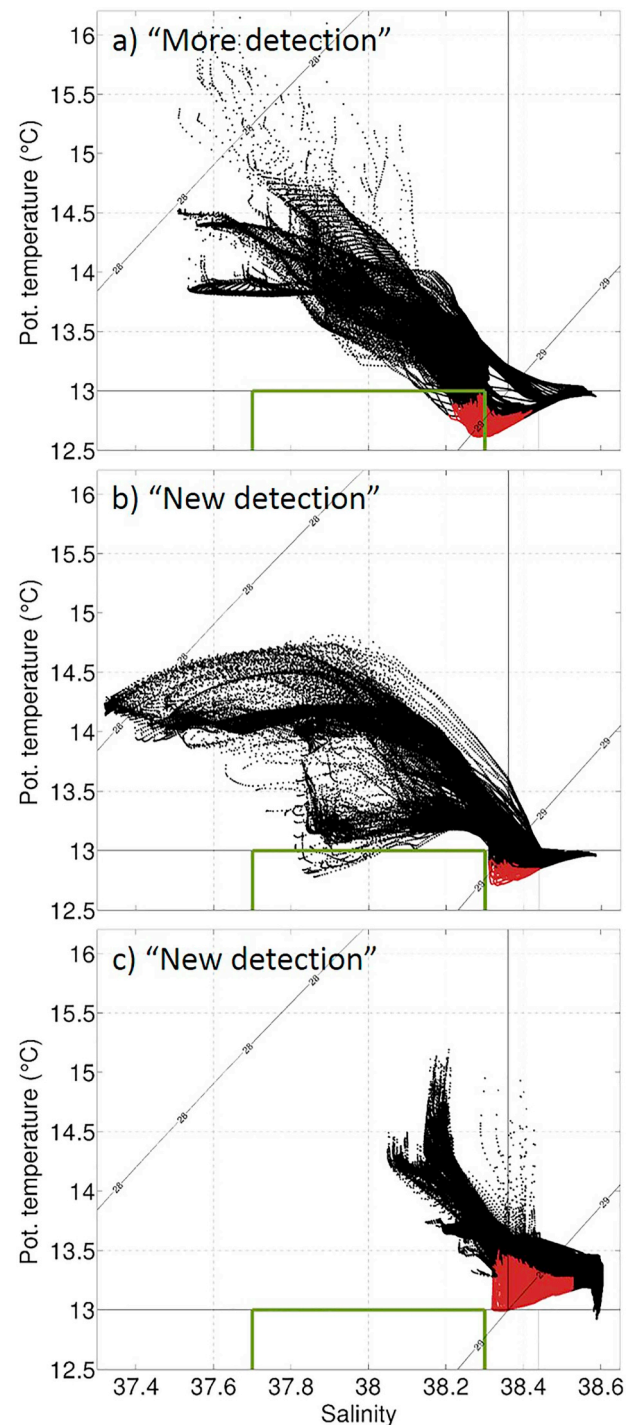


Fig. 4. θ/S diagrams from model during the missions in March 2011 (a), February 2011 (b) and March 2015 (c). The missions a), b) and c) depict the two types of detection results found in model data.

5.2. Evolution of the basin-wide volume

The fixed-range and geometry-based criteria are also applied to the four-dimensional WMOP simulation to compare the WIW detection methods at basin-scale. A larger volume of WIW is captured in the WMED from 2011 to 2015 with the geometric method compared to the fixed-range criterion (Fig. 5). This latter mainly detects WIW which is located in the plateau of GoL and the Ebro delta region. Although WIW is also detected in the open ocean of the Ligurian Sea in 2011 and 2012, very few WIW θ/S value is captured in 2014 and 2015. On the contrary,

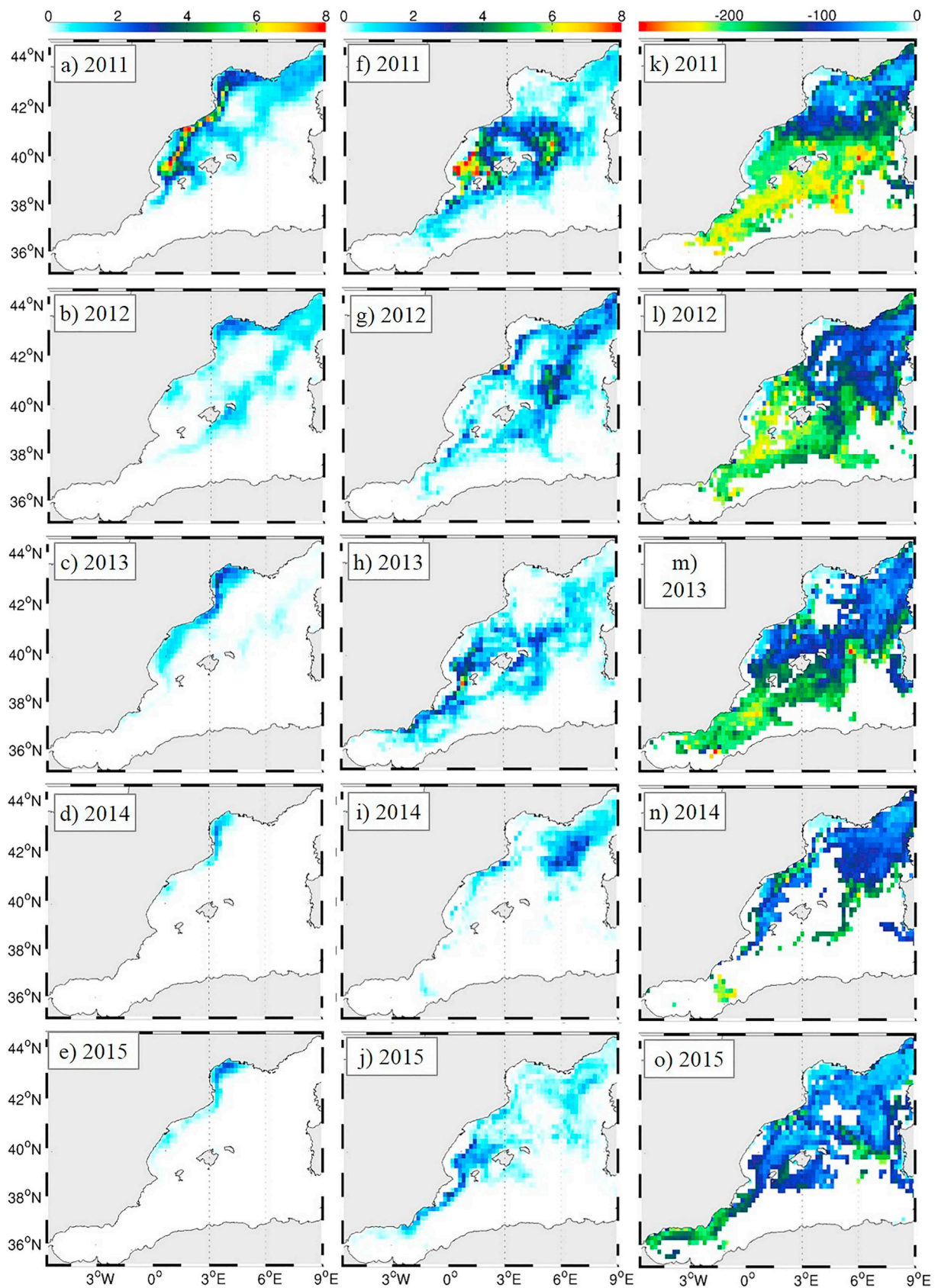


Fig. 5. Cumulated annual volume (in $10^{12} \times \text{m}^3$) of WIW as detected in WMOP in box of $0.2^\circ \times 0.2^\circ$ over 2011–2015 by the fixed-range (a–e) and geometric (f–j) criteria and associated depth median (in m) for the geometric one (k–o).

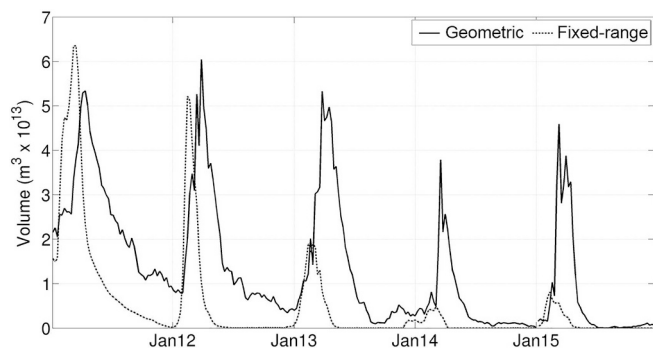


Fig. 6. Volume (in m^3) of weekly WIW in the WMED as detected by the fixed-range and geometric criteria in WMOP from 2011 to 2015.

the geometric method captures WIW from the Ligurian Sea to the south of the Balearic Islands and the Alboran Sea. The geometry-based criterion detects a volume of WIW which is larger locally and more extended in the basin every year.

The time series of the volume integrated within the whole domain (Fig. 6) also clearly show the larger amount of WIW detected at basin scale with the geometric detection. The peaks, which occur in winter-time when WIW is formed, are generally higher and larger with the new method. This latter also detects WIW throughout almost the whole period from 2011 to 2015. The weekly resolution highlights a temporal shift between WIW maxima detected with the two methods, which probably corresponds to exact timing of WIW formation, when all AW is convected (leading to the absence of AW in the θ/S diagram restricting the WIW detection with the geometric method) and the difference in location of detected WIW. Finally, while Fig. 5 highlights temporal and spatial variations in WIW detection with both methods, Fig. 6 reveals the weekly, seasonal and interannual variability at basin scale. Further investigations of the temporal and spatial variability of the WIW characteristics are addressed in the next section.

6. Spatio-temporal variability in WIW characteristics

In this section, the geometric method is applied to glider data as well as the interpolated and fully-sampled model outputs to investigate the spatio-temporal changes in WIW properties.

6.1. Temporal evolution in the Ibiza Channel

Time series of the medians of WIW θ and S distributions over each mission are depicted (Fig. 7) to outline the presence of WIW and the temporal evolution of its hydrographic properties as captured by the glider data and interpolated WMOP in the IC. In both datasets, the presence of WIW is seasonal: this water mass is mainly captured during the missions in winter-spring. Fig. 7 also clearly shows how both limits in θ and S of the fixed-range criterion are not adequate to capture properly WIW over the period of study: θ medians are warmer than 13°C from 2015 to 2017 while S medians are saltier than 38.3 in 2012–2013 and 2016–2017.

The WIW θ seems to have a seasonal variability with minimum generally reached in March. The minimum of median value is observed in March 2011 (12.8°C). Year-to-year variability is also highlighted in glider data with medians varying between 12.8 and 13°C over 2011–2013, and higher values found over 2015–2017 (13.1 – 13.4°C). WMOP produces WIW in the IC when it is observed. The simulation is able to reproduce both the observed seasonal and interannual variations of WIW θ , as well as the minimum found in March 2011 and the warmest WIW in winter-spring 2015. The glider (model) WIW θ median values vary from 12.8 to 13.2°C (12.7 to 13.3°C) from 2011 to 2015. The simulation covers a wider range of θ since it underestimates (overestimates) θ in 2011 (2015) leading to an overestimation of the

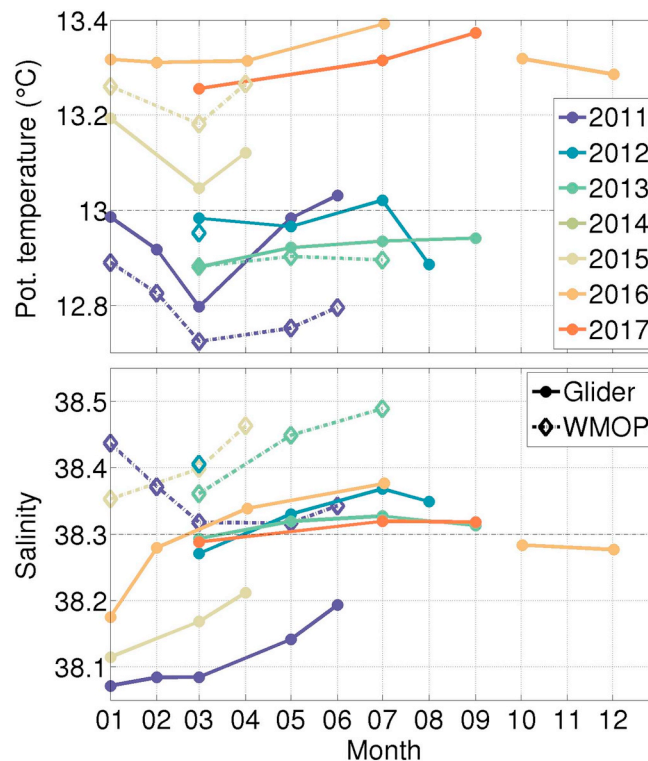


Fig. 7. Time series of the medians of WIW θ (top) and S (bottom) distributions over each mission in the IC from gliders over 2011–2017 (solid lines) and interpolated simulation over 2011–2015 (dashed lines). The horizontal lines indicate the θ and S limits of the fixed-range criterion (13°C and 38.3, respectively).

warming rate.

Seasonal variations in WIW S with minimum in winter and maximum in summer are partially observed in the IC. Year-to-year variability is also captured with minima observed in 2011 and 2015 (38.1 – 38.2) and maxima in 2012 and 2016 (38.3 – 38.4). WIW is saltier in WMOP than in observations. The glider (model) WIW S oscillates between 38.1 and 38.35 (38.3 and 38.5) over the period 2011–2015. The model overestimation (0.1 – 0.3) is persistent over the whole investigated period. This model S shift involves the whole water column as shown in the θ/S diagrams from the glider and interpolated model data in the IC in February 2011 (Figs. 3a and 4b) and in March 2015 (Figs. 3c and 4c). Despite this model error, the seasonal and interannual variability of WIW S is reproduced in WMOP, although the interannual variations are smaller than in the observations.

In conclusion, these results show that the simulated seasonal and interannual variability of the WIW properties in the IC is in agreement with the observations despite the above-mentioned model errors. Hence, the fully-sampled model is now used to follow the continuous temporal evolution of the WIW in the IC as well as the regional variations in the adjacent sub-basins, keeping in mind the model biases.

The temporal evolution of the WIW properties is analysed using the fully-sampled model in the section at 39°N (Fig. 8), which corresponds to the glider endurance line (Fig. 1). It highlights changes in θ and S from monthly to interannual time scales in the IC. WIW is present almost all the months in the fully-sampled model while it was not always detected in the interpolated model (Fig. 7). Indeed, the temporally even and spatially complete coverage of the section in the fully-sampled dataset allows to catch some relatively mixed WIW (i.e. with less marked θ minima) particularly in fall. This modified WIW is present in smaller quantities than during the months of formation and recent propagation (not shown).

Marked seasonal variability in WIW θ and S is reproduced in the

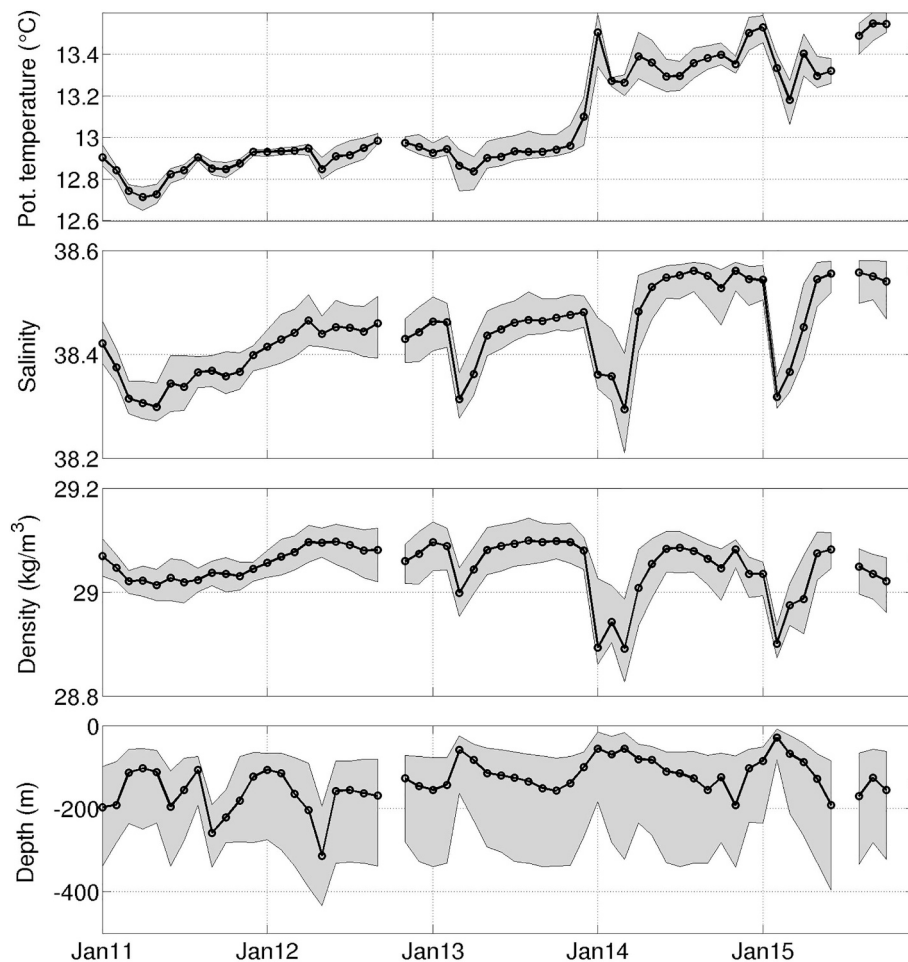


Fig. 8. Medians (black lines), 17 and 83th percentiles (delimited by the shadow area) of the monthly distributions of WIW θ , S, σ and depth (from top to bottom) from the fully-sampled model along the IC section from 2011 to 2015.

simulation, with minima generally found in end-winter or early-spring. WIW occupies shallow layers in wintertime due to recent formation. The year 2012 is exceptional with relatively constant θ and S median values throughout the year and the 17th percentile of depth not close to the surface indicating that WIW is not recently formed. Concerning the year-to-year variability, a strong increase in WIW θ is detected since January 2014. In 2013–2014–2015, strong and abrupt S minima in winter associated with shallow depths suggest that the detected WIW is recently formed in the plateau of the Ebro delta region. These years are also associated with an enlargement of the WIW layer due to accumulation of WIW which is recently formed and WIW originating from the north WMED. The WIW density anomaly (σ) reaches its minima in winters 2014 and 2015 when WIW is particularly warm and fresh during its formation process. In conclusion, the model suggests the presence of recently formed WIW in the IC coming from the north WMED and the Ebro delta region in wintertime, as well as some relatively mixed WIW the rest of the year. Changes in WIW properties are also simulated, in particular a strong increase in θ since 2014.

6.2. Spatio-temporal variability in the western Mediterranean

The analyses are extended to the four selected sections (displayed in Fig. 1) to follow the temporal and regional variations of WIW properties (Fig. 9). Beside the S overestimation in the model (Section 6.1), the θ /S maxima associated with LIW is not well marked in the simulation due to the particularly flattened θ maximum (as noticeable in Fig. 4). This model feature does not prevent the method detecting properly the LIW position (and then WIW). Nevertheless, the difference between

simulated WIW and LIW θ is small particularly in summer-fall, i.e. outside of the WIW formation period (when the θ minimum is less marked). Due to the more homogeneous surface and intermediate layer in the simulation, this latter also catches modified and mixed WIW with surrounding waters in the studied sections.

In the north-eastern GoL, the simulated WIW θ and S have a relatively large seasonal variability with median value minima and largest distributions found in winter when strong atmospheric events and WIW formation occur. While the WIW θ oscillates annually from 12.6 to 13.4 °C from 2011 to 2013, it is warmer in 2014 and 2015 with median values around 13.5 °C throughout the year. Note that this warming is not associated with shallower depths nor significant density changes (not shown) since S is also increasing. The depth minima are also found in winter due to surface WIW which is recently formed or being formed. The 17th percentile is close to the surface during all winter months of the period (not shown). In early-winter, the volume of WIW (represented in Fig. 9 by the mean surface along the section) is equal to 0 when all AW is being transformed into WIW. Then, the largest amount is generally found in late-winter when recently formed WIW is detected (associated with an increased horizontal extension in shallow depths), and in end-summer when WIW previously formed in the Ligurian Sea and GoL has recirculated crossing the section. In summer-fall, WIW flows below AW reaching its depth maxima.

In the south-western GoL, the simulation suggests that the WIW characteristics also have a seasonal variability with θ (S) tending to be colder (saltier) than in the north-eastern GoL. The WIW volume is also equal to 0 during the formation process in early-winter and reaches its maxima in March–April when a large amount of recently formed WIW

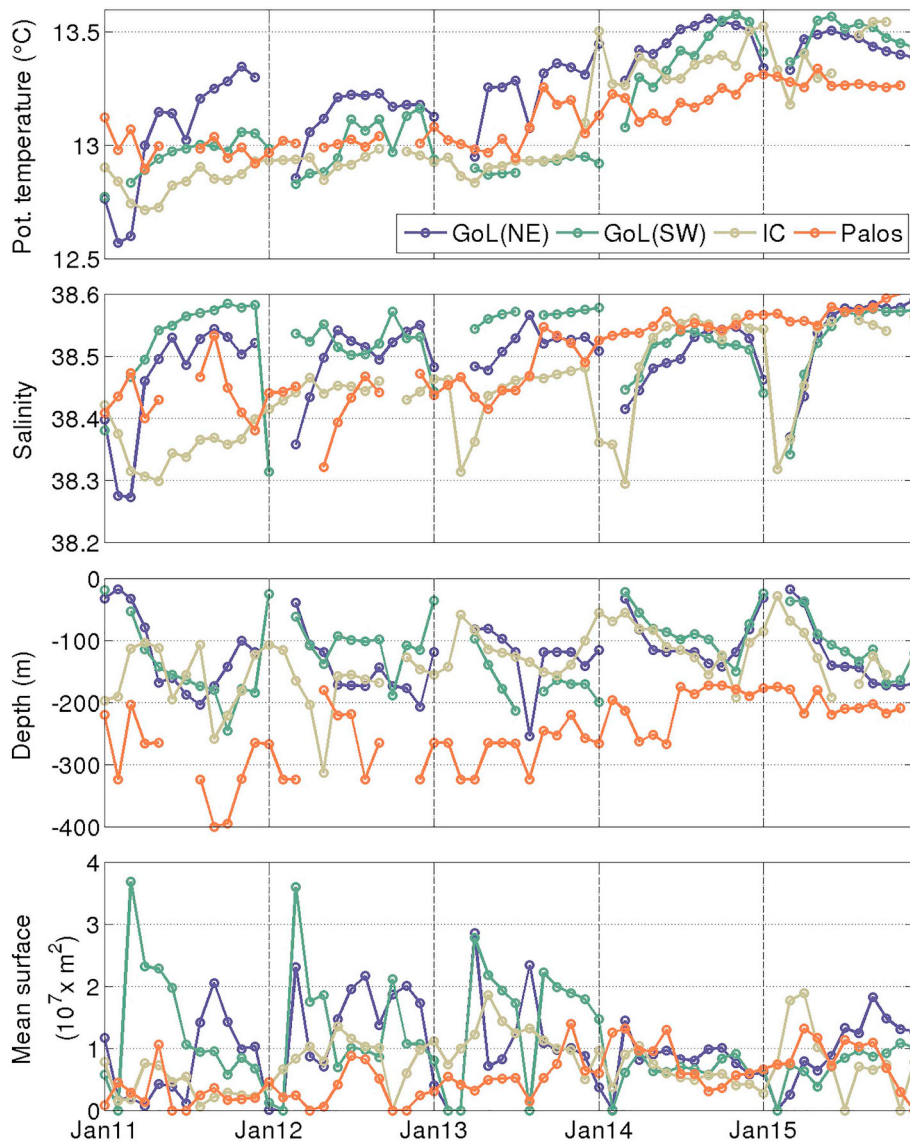


Fig. 9. Medians of the monthly distributions of WIW θ , S and depth, and monthly mean of surface with WIW (from top to bottom) from the fully-sampled model along the four sections (indicated in Fig. 1) from 2011 to 2015.

is detected (particularly in 2011, 2012 and 2013), with values higher than in the north-eastern GoL. Peaks of WIW volume are also reached, especially in falls 2012 and 2013, in deeper layer than in winter, due the presence of recirculated WIW. The spatial changes in simulated WIW characteristics between the two sections of GoL suggest the addition of WIW formed in the continental plateau and in GoL. Note also that the formation of WIW in GoL is smaller in 2014 and 2015 than in previous years.

Further south, in the IC, WIW tends to be warmer (colder) in winter (summer-fall) than in the south-western GoL. WIW is clearly fresher and occupies shallower water in winter. The θ and S seasonal variability clearly persists with minima in late-winter and early-spring, associated with depth minima (Section 6.1), with 1–2 month delay with GoL. Additionally, the model produces a larger volume of WIW from February to May 2015 in IC than in GoL during the previous and synchronous months. That clearly indicates the convection forming WIW in the plateau of the Ebro delta region.

Approaching the Alboran Sea, the θ minimum is less marked than in the northern regions but still appears in the θ /S diagrams certifying the presence of WIW. The properties have lost their seasonal variability, getting distance from the formation area and mixing with surrounding

water masses. WIW is deeper than in GoL and the Balearic Sea (the 17th percentile is not close to the surface) pointing out the horizontal and vertical propagation. Additionally, the medians of WIW depth at Cape Palos oscillate around 300 m (200 m) over 2011–2013 (2014–2015) with the 5th percentile varying around 200 m (100 m) (not shown). Hence, according to the model results, WIW could contribute to the Mediterranean outflow at the Strait of Gibraltar, of which the shallowest point is located at 300 m depth (Camarinal Sill).

In summary, the time series of simulated regional WIW characteristics (Fig. 9) associated with the annual maps of WIW volume and depth from 2011 to 2015 (Fig. 5f–o) clearly suggest the significant interannual variations in WIW formation site, as well as the horizontal and vertical propagation over the WMED. In 2011 and 2012, the shallow depths with median values between 0 and 50 m, which indicate the WIW formation site(s), are mainly found in the Ligurian Sea and GoL (Fig. 5k, l). Shallow depths extend to the Balearic Sea in 2013 and 2015. During these years, a large volume is found in this region crossing the IC, and reaching the Alboran Sea and the Strait of Gibraltar (Fig. 5m, o). The southward propagation from the formation site is joined with a deepening with median values reaching 250 m in the southern basin. The changes in simulated WIW characteristics (θ , S and

Table 2

Trends significant at the 90% level (Chelton, 1983) of WIW and LIW θ (in °C/year), S (in /year) and σ (in kg/m³/year) from the fully-sampled model in the four sections (displayed in Fig. 1) over the period 2011–2015.

	WIW θ	WIW S	WIW σ	LIW θ	LIW S	LIW σ
GoL(NE)	0.12 ± 0.006	0.02 ± 0.002	–	0.06 ± 0.005	0.01 ± 0.0005	–
GoL(SE)	0.14 ± 0.006	–	–0.027 ± 0.002	0.15 ± 0.007	0.006 ± 0.0006	–0.028 ± 0.0015
IC	0.16 ± 0.005	0.04 ± 0.003	–0.005 ± 0.002	0.11 ± 0.006	0.01 ± 0.0009	–0.015 ± 0.0007
Palos	0.07 ± 0.002	0.04 ± 0.002	0.015 ± 0.0006	–	–	–

Table 3

Trends with 90% confidence level (Chelton, 1983) of the LIW θ (in °C/year), S (in /year) and σ (in kg/m³/year), from collocated WMOP and gliders for the missions from 2011 to 2017 in the IC.

	LIW θ	LIW S	LIW σ
WMOP 2011–2015	0.1 ± 0.007	0.02 ± 0.001	–0.006 ± 0.0007
Gliders 2011–2015	0.05 ± 0.007	0.008 ± 0.002	–0.005 ± 0.001
Gliders 2011–2017	0.04 ± 0.004	0.009 ± 0.0007	–0.002 ± 0.0003

depth) could be related to the formation site and the horizontal and vertical propagation but not only since no correlation is found between the spatial pattern of θ , S and depth maps (supplementary material A). The WIW θ increases in the whole domain from the Ligurian Sea to the Alboran Sea in 2014 and 2015, while the S increase is neither homogeneous nor related to the WIW depth and volume (supplementary material A).

7. Trends in the western Mediterranean

7.1. Regional trends

Linear regressions from the monthly WIW characteristics time series depict positive trends in both θ and S in the four sections of the WMED (Table 2). The simulated WIW is warmer in the Alboran Sea than in the IC in 2011, 2012 and 2013 while they become colder in 2014 and 2015 leading to a smaller trend in θ in Cape Palos. The WIW θ increase affects more GoL and the Balearic Sea than the Alboran Sea while the WIW S increase is larger in the Alboran and Balearic Seas than in GoL. Remember that simulation errors have been found in θ and S comparing to observations (Section 6.1). In particular, the θ trend is overestimated over the studied period in the IC: the simulated WIW and LIW θ trends (around 0.1 °C/year) are more than twice the observed ones. Additionally, these trends are computed over 5 and 7-year periods and therefore may be part of the interannual or decadal variability. Note that the glider instrument stability has approximately one order of magnitude less than the monthly WIW characteristics which are used to compute the observed trends, thus not impacting on their estimates.

Through its impact on the density, the ocean warming could prevent the convection until the intermediate layer and restrict the WIW formation. However, the concomitant increase of S balances partially the effect of θ changes on the density. The monthly WIW σ is correlated to the S variability in the four sections, north-eastern and south-western GoL, IC and Cape Palos (with correlations around 0.51, 0.64, 0.55 and 0.9, respectively) while the WIW warming induces a decrease in density. The model suggests that the σ trends are negative in GoL and IC (Table 2) while in Cape Palos, where the θ (S) trend is less (more) important than in the further north regions, the σ trend is positive. These slight changes in density in the north WMED are not accompanied by significant changes in depth, except for the year 2014 when less dense and shallower WIW is found throughout the year due to the general warming.

7.2. Warming and salting: discussion

WIW is formed through intense cooling and vertical mixing of AW. The θ trends may result from the greenhouse-gas-induced warming in the WMED (Bethoux et al., 1990). The reduction in fresh water inputs (via river damming and decrease of precipitations) may be the major cause of the S increase in surface waters that can induce salting of intermediate and deep waters through surface waters cooling in winter (Krahmann and Schott, 1998; Schroeder et al., 2006; Skliris et al., 2007). Additional cause of the hydrographic changes of WIW could be the changes of the inflowing AW (Millot et al., 2006). Changes in LIW properties (Ben Ismail et al., 2014; Vargas-Yáñez et al., 2017; Schroeder et al., 2017), that could be related to atmospheric events and/or mixing process during its route from the EMED, can also affect the WIW formation. Denser LIW would make the deep convection more difficult and more WIW could be formed, and vice versa. During the WIW detection procedure, as a first stage, LIW is identified finding the θ maximum in the 95–99th percentile range of S, i.e. in the LIW core. The temporal evolution of LIW properties across the sections can also be easily outlined. Despite the persistent model errors in θ and S maxima associated with LIW, similar behaviour in θ , S and σ trends are found with gliders data in the IC (Table 3). The trends of LIW θ and S are positive in both glider and model data as captured during the missions from 2011 to 2015, leading to a negative trend in σ . Extending the period to 2017 with glider measurements, the trends demonstrate lower values in θ and higher ones in S reducing the negative trend in σ .

The trends in θ , S and σ for both WIW and LIW have been computed in the four sections (analysed in Section 6.2) using the fully-sampled model (Table 2). This points out the similar behaviour of both water masses in the Balearic Sea and GoL. The model suggests that the positive trends in θ and S lead to negative trend in σ for both WIW and LIW in the north WMED. Less dense WIW and LIW would induce more homogeneous surface and intermediate layers reducing their stability. The decrease of density hinders any further outflow sinking (Schroeder et al., 2006). The decrease in surface density and in winter deep water formation could thus induce the weakening of the Mediterranean thermohaline circulation. The hydrographic properties of the Mediterranean Outflow Water flowing into the Atlantic Ocean would be strongly influenced by these changes (Somot et al., 2006). Their modifications could in turn modify the heat and salt content of the Atlantic Ocean (Curry et al., 2003) and influence its thermohaline circulation.

8. Conclusions and perspectives

While hydrographic changes of LIW and WMDW, in particular their warming and salting, have been largely addressed, the evolution of WIW characteristics is poorly documented. In this paper, we propose an innovative geometric criterion to detect WIW in the western Mediterranean Sea (WMED) from the θ /S diagram shape, allowing to track the spatio-temporal changes in temperature and salinity properties.

The fixed-range method is based on pre-determined temperature and salinity ranges. Hence, changes in WIW properties (e.g. increase of temperature) which are out of the ranges would be interpreted as absence or loss of this water mass. To overcome this issue, a geometry-

based criterion has been developed taking advantage of the position of WIW between surface waters and LIW with temperature minima. This method enables to detect changes in WIW properties and, in particular, to catch larger amount of WIW with higher temperature and salinity. Considering the glider missions in the Ibiza Channel from 2011 to 2017 when WIW has been detected in observations by the geometric method, 36% of cases correspond to more WIW θ/S values detected compared to the fixed-range criterion while 56% are new detections. Due to model biases (particularly in salinity), 33% of the WIW detections in the simulation are associated with more WIW detected with the geometric method and 67% with new detections thanks to the geometric criterion. The new criterion is able to cope with model biases and detect the presence of WIW.

The detection resulting from the geometric criterion shows seasonal and year-to-year variability in WIW properties as captured by the gliders from 2011 to 2017 in the Ibiza Channel. The most marked feature in WIW changes over the last seven years is the abrupt warming in 2015 with temperature higher than 13 °C (with median values between 13.2 and 13.4 °C). Although model errors are found in temperature and salinity, the simulation is able to reproduce the observed presence or absence of WIW in the channel, as well as the winter temperature minima, the abrupt warming in 2015 or the fresher salinity in winter. The evaluation of WMOP model in the Ibiza Channel gives us confidence in using the continuous time series from the simulation in different key sections of the WMED to study the spatio-temporal evolution of WIW characteristics.

The fully-sampled simulation suggests the seasonal cycle of WIW temperature and salinity in the Gulf of Lion and Balearic Sea, as well as of WIW depth with minima reached when WIW is recently formed. WIW propagates southwards from the formation site(s) to the Alboran Sea with deepening of the occupation layer. According to the WMOP simulation, WIW is mainly formed in the Ligurian Sea and the Gulf of Lion in 2011 and 2012. The Balearic Sea becomes an important additional WIW formation site particularly in 2013 and 2015 with a large annual cumulated volume of WIW. During these years, the simulated WIW reaches the Strait of Gibraltar. Positive trends in simulated WIW temperature and salinity appear in all the studied sections, from the Gulf of Lion to the Alboran Sea. The results from the simulation indicate that WIW temperature (salinity) in the WMED are increasing at a rate of 0.07–0.15 °C/year (0.003–0.04/year) from 2011 to 2015. Analyses of regional properties using the basin-scale numerical simulation have also suggested the spatial variability of WIW characteristics in the WMED, due to the formation sites, horizontal and vertical propagations, and mixing with surrounding waters.

The LIW changes have been also detected through the first step of the WIW detection method. Both simulated temperature and salinity have shown an increasing trend for WIW and LIW, with similar behaviour in the three sections of the north WMED. The concomitant increases of temperature and salinity, which have opposite effects on density, are not totally balanced, leading to slight decreases in density and depths, in the main formation and propagation areas (Gulf of Lion and Balearic Sea). At the entrance of the Alboran Sea, at Cape Palos, a positive trend in density is detected by the model for both WIW and LIW.

As discussed in the paper, some quantifications should be considered with caution. The study covers a limited period. Additionally, the numerical simulations are subject to systematic errors induced by several model factors: unresolved or parameterized physical processes, numerical schemes, inaccurate initial conditions, errors in atmospheric forcings, air-sea flux uncertainties, and river runoff approximations.

This study demonstrates the capability of this innovative geometry-based criterion to automatically adjust to changes in WIW properties. This approach can also detect the presence of simulated WIW in case of model biases and it could be applied operationally to near real-time (not calibrated) observations that may include salinity shift. As the traditional fixed-range criterion, the proposed method uses parameters,

but which are much less restrictive. It allows to detect properly the WIW properties in both glider and model data, in the Ibiza Channel and the whole WMED, capturing both temporal and spatial changes. However, the fixed-value parameters might limit the detection in the future due to new unexpected changes in water mass properties and/or different model characteristics and errors. To remove this constraint, the local stratification might be determined and introduced in the detection procedure replacing these parameters. Moreover, this method requires a three-layer system, comprising the typical surface and intermediate water masses of the WMED (AW, WIW, and LIW). It has been adapted to catch the recently formed WIW, but the water mass cannot be detected locally during the formation process due to the absence of AW, which is entirely transformed into WIW. This restriction might be overcome by using the geographical position and characteristics of the identified recently formed WIW and looking for similar temperature and salinity values during the previous days in a surfacing homogeneous vertical layer of the region. Additionally, a minimum of profiles in the θ/S diagram is required since the method uses distribution properties of an ensemble of profiles (e.g. percentiles). Dense data (e.g. from gliders and models) are therefore particularly adapted for local detection from daily/weekly to longer time scales. Temporally and spatially sparse data (e.g. from Argo floats) should be congregated for regional analyses from seasonal to longer time scales.

The analyses could be extended over the last decades applying the geometry-based method to long-term datasets. Regular observations and/or simulations over a longer period could help to understand the spatio-temporal variability in water mass properties, to determine the time scales of variability (interannual, decadal or trend) and the ocean response to climate change. Finally, further investigations about the causes of WIW changes (e.g. changes in atmospheric conditions, inflowing AW, and water column properties including changes in LIW) and their respective contributions could be addressed taking advantage of the proposed method. Hence, consequences might be better identified and quantified, such as changes in water column properties, modifications in the stratification that can affect the convection events, or changes in density of the intermediate layer and in the Mediterranean Outflow Water, which directly impacts the Meridional Overturning Circulation and the ocean climate system.

Glossary

AW	Atlantic Water
ρ	Density
IC	Ibiza Channel
EMED	Eastern Mediterranean Sea
LIW	Levantine Intermediate Water
MOW	Mediterranean Outflow Water
NC	Northern Current
S	Salinity
T	Temperature
θ	Potential temperature
σ	Density anomaly
SOCIB	Balearic Islands Coastal Observing and forecasting System
WIW	Western Intermediate Water
WMDW	Western Mediterranean Deep Water
WMED	Western Mediterranean Sea
WMOP	Western Mediterranean Operational system

Acknowledgments

We gratefully acknowledge the two anonymous reviewers for their relevant remarks. The study has been conducted using glider data, which are post-processed and distributed by the SOCIB Data Centre team.

Appendix A. Supplementary data

Supplementary data to this article can be found online at <https://doi.org/10.1016/j.jmarsys.2018.11.003>.

References

- Amores, A., Montserrat, S., Marcos, M., 2013. Vertical structure and temporal evolution of an anticyclonic eddy in the Balearic Sea (western Mediterranean). *J. Geophys. Res.* 118 (4), 2097–2106. <https://doi.org/10.1002/jgrc.20150>.
- Astraldi, M., Balopoulos, S., Candela, J., Font, J., Gacic, M., Gasparini, G.P., Manca, B., Theocharis, A., Tintoré, J., 1999. The role of straits and channels in understanding the characteristics of Mediterranean circulation. *Prog. Oceanogr.* 44, 65–108.
- Ben Ismail, S., Schroeder, K., Sammari, C., Gasparini, G.P., Borghini, M., Aleya, L., 2014. Interannual variability of water mass properties in the Tunisia-Sicily Channel. *J. Mar. Syst.* 135, 14–28. <https://doi.org/10.1016/j.jmarsys.2013.06.010>.
- Bethoux, J.P., Gentili, B., Raunet, J., Tailliez, D., 1990. Warming trend in the western Mediterranean deep water. *Nature* 347, 660–662.
- Bethoux, J.P., Gentili, B., Morin, P., Nicolas, E., Pierre, C., Ruiz-Pino, D., 1999. The Mediterranean Sea: a miniature ocean for climatic and environmental studies and a key for the climatic functioning of the North Atlantic. *Prog. Oceanogr.* 44, 131–146.
- Borghini, M., Bryden, H., Schroeder, K., Sparnocchia, S., Vetrano, A., 2014. The Mediterranean is becoming saltier. *Ocean Sci.* 10, 693–700. <https://doi.org/10.5194/os-10-693-2014>.
- Candela, J., 2001. Chapter 5.7. Mediterranean water and global circulation. *Int. Geophys.* 77 [https://doi.org/10.1016/S0074.6142\(01\)80132-7](https://doi.org/10.1016/S0074.6142(01)80132-7). ISSN 0074-6142.
- Chelton, D.B., 1983. Effects of sampling errors in statistical estimation. *Deep Sea Res. Part A* 30 (10), 1083–1103.
- Curry, R., Dickson, B., Yashayaev, I., 2003. A change in the freshwater balance of the Atlantic Ocean over the past four decades. *Nature* 426 (6968), 826.
- Fairall, C.F., Bradley, E.F., Hare, J.E., Grachev, A.A., Edson, J.B., 2003. Bulk parameterization of air-sea fluxes: updates and verification for the COARE algorithm. *J. Clim.* 16, 571–591. [https://doi.org/10.1175/1520-0442\(2003\)016<0571:BPOASF>2.0.CO;2](https://doi.org/10.1175/1520-0442(2003)016<0571:BPOASF>2.0.CO;2).
- García-Martínez, C., Vargas-Yáñez, M., Moya, F., Zunino, P., Bautista, B., 2018. The effects of climate change and rivers damping in the Mediterranean during the twentieth century. *Res. J. Environ. Sci.* <https://doi.org/10.19080/IJESNR.2018.08.555741>.
- Heslop, E.E., Ruiz, S., Allen, J., López-Jurado, J.L., Renault, L., Tintoré, J., 2012. Autonomous underwater gliders monitoring variability at “choke points” in our ocean system: a case study in the Western Mediterranean Sea. *Geophys. Res. Lett.* 39.
- Houperl, L., Durrieu de Madron, X., Testor, P., Bosse, A., D’Ortenzio, F., Bouin, M.N., Dausse, D., Le Goff, H., Kunesch, S., Labaste, M., Coppola, L., Mortier, L., Raimbault, P., 2016. Observations of open-ocean deep convection in the north-western Mediterranean Sea: seasonal and interannual variability of mixing and deep water masses for the 2007–2013 period. *J. Geophys. Res. Oceans* 121, 8139–8171. <https://doi.org/10.1002/2016JC011857>.
- Juza, M., Renault, L., Ruiz, S., Tintoré, J., 2013. Origin and pathway of winter intermediate water in the Northwestern Mediterranean Sea using observations and numerical simulation. *J. Geophys. Res.* 118, 1–13. <https://doi.org/10.1002/2013JC009231>.
- Juza, M., Murre, B., Renault, L., Gómara, S., Sebastián, K., Lora, S., Beltran, J.P., Frontera, B., Garau, B., Troupin, C., Torner, M., Heslop, E., Casas, B., Escudier, R., Vizoso, G., Tintoré, J., 2016. SOCIB operational ocean forecasting system and multi-platform validation in the Western Mediterranean Sea. *J. Oper. Oceanogr.* 9, s155–s166.
- Krahmann, G., Schott, F., 1998. Longterm increases in western Mediterranean salinity and temperatures: anthropogenic and climate sources. *Geophys. Res. Lett.* 25 (22), 4209–4212. <https://doi.org/10.1029/1998GL900143>.
- López-Jurado, J., Lafuente, J.M.G., Lucaya, N.C., 1995. Hydrographic conditions of the Ibiza Channel during November 1990, March 1991 and July 1992. *Oceanol. Acta* 18 (2), 235–243.
- Malanotte-Rizzoli, P., Artale, V., Borzelli-Eusebi, G.L., Brenner, S., Crise, A., Gacic, M., Kress, N., Marullo, S., Ribera d’Alcalá, M., Sofianos, S., Tanhua, T., Theocharis, A., Alvarez, M., Ashkenazy, Y., Bergamasco, A., Cardin, V., Carniel, S., Civitarese, G., D’Ortenzio, F., Font, J., Garcia-Ladona, E., Garcia-Lafuente, J.M., Gogou, A., Gregoire, M., Hainbucher, D., Kontoyannis, H., Kovacevic, V., Kraskapoulou, E., Kroskos, G., Incarbona, A., Mazzochi, M.G., Orlic, M., Ozsoy, E., Pascual, A., Poulain, J.M., Roether, W., Rubino, A., Schroeder, K., Siokou-Frangou, J., Souvermezoglou, E., Sprovieri, M., Tintoré, J., Triantafyllou, G., 2014. Physical forcing and physical/biochemical variability of the Mediterranean Sea: a review of unresolved issue and directions for future research. *Ocean Sci.* 10, 281–322. <https://doi.org/10.5194/os-10-281-2014>.
- Marty, J.C., Chiavérini, J., 2010. Hydrological changes in the Ligurian Sea (NW Mediterranean; DYFAMED site) during 1995–2007 and biogeochemical consequences. *Biogeosciences* 7 (7), 2117–2128. <https://doi.org/10.5194/bg-7-2117-2010>.
- Millot, C., 1999. Circulation in the Western Mediterranean Sea. *J. Mar. Syst.* 20, 423–442.
- Millot, C., Taupier-Letage, I., 2005. Circulation in the Mediterranean Sea. The Mediterranean Sea. Springer, Berlin Heidelberg, pp. 29–66.
- Millot, C., Candela, J., Fuda, J.L., Tber, Y., 2006. Large warming and salinification of the Mediterranean outflow due to changes in its composition. *Deep Sea Res., Part I* 53, 656–666. <https://doi.org/10.1016/j.dsr.2005.12.017>.
- Mourre, B., Aguiar, E., Juza, M., Hernandez-Lasheras, J., Reyes, E., Heslop, E., Escudier, R., Cutolo, E., Ruiz, S., Mason, E., Pascual, A., Tintoré, J., 2018. Assessment of high-resolution regional ocean prediction systems using multi-platform observations: illustrations in the western Mediterranean Sea. In: Chassignet, E., Pascual, A., Tintoré, J., Verron, J. (Eds.), *New Frontiers in Operational Oceanography*. GODAE OceanView, pp. 663–694. <https://doi.org/10.17125/gov2018.ch24>.
- Pinot, J.M., Ganachaud, A., 1999. The role of winter intermediate waters in the spring-summer circulation of the Balearic Sea. *J. Geophys. Res.* 104 (C12), 29843–29864.
- Pinot, J.M., Tintoré, J., Gomis, D., 1995. Multivariate analysis of the surface circulation in the Balearic Sea. *Prog. Oceanogr.* 36 (4), 343–376.
- Pinot, J.M., López-Jurado, J.L., Riera, M., 2002. The CANALES experiment (1996–1998). Interannual, seasonal, and mesoscale variability of the circulation in the Balearic channels. *Prog. Oceanogr.* 55, 335–370.
- Reid, J.L., 1979. On the contribution of the Mediterranean Sea outflow on the Norwegian-Greenland Sea. *Deep-Sea Res.* 26A, 1199–1223.
- Robinson, A.R., Leslie, W.G., Theocharis, A., Lascaratos, A., 2001. Mediterranean sea circulation. In: *Ocean Currents: A Derivative of the Encyclopedia of Ocean Sciences*. vol. 3. Academic, London, pp. 1689–1705. <https://doi.org/10.1006/rwos.2001.0376>.
- Salat, J., Font, J., 1987. Water mass structure near and offshore the Catalan coast during the winter of 1982 and 1983. *Ann. Geophys.* 5, 49–54.
- Salat, J., Puig, P., Latasa, M., 2010. Violent storms in the sea: dense water formation episodes in the NW Mediterranean. *Adv. Geosci.* 26, 53–59. <https://doi.org/10.5194/adgeo-26-53-2010>.
- Schroeder, K., Gasparini, G.P., Tangherlini, M., Astraldi, M., 2006. Deep and intermediate water in the western Mediterranean under the influence of the Eastern Mediterranean Transient. *Geophys. Res. Lett.* 33, L21607. <https://doi.org/10.1029/2006GL027121>.
- Schroeder, K., Chiggiato, J., Bryden, H.L., Borghini, M., Ben Ismail, S., 2016. Abrupt climate shift in the western Mediterranean Sea. *Sci. Rep.* 6 (23009). <https://doi.org/10.1038/srep23009>.
- Schroeder, K., Chiggiato, J., Josey, S.A., Borghini, M., Aracri, S., Sparnocchia, S., 2017. Rapid response to climate change in a marginal sea. *Sci. Rep.* 7 (4065). <https://doi.org/10.1038/s41598-017-04455-5>.
- Send, U., Font, J., Krahmann, G., Millot, C., Rhein, M., Tintoré, J., 1999. Recent advances in observing the physical oceanography of the western Mediterranean Sea. *Prog. Oceanogr.* 44, 37–64.
- Shchepetkin, A.F., McWilliams, J.C., 2003. A method for computing horizontal pressure-gradient force in an oceanic model with a nonaligned vertical coordinate. *J. Geophys. Res.* 108 (C3).
- Shchepetkin, A.F., McWilliams, J.C., 2005. The regional oceanic modeling system (ROMS): a split explicit, free-surface, topography-following-coordinate oceanic model. *Ocean Model* 9, 347–404.
- Simoncelli, S., Fratanni, C., Pinardi, N., Grandi, A., Drudi, M., Oddo, P., Dobricic, S., 2014. Mediterranean Sea physical reanalysis (MEDREA 1987–2015) (Version 1). In: E.U. Copernicus Marine Service Information, https://doi.org/10.25423/medsea_reanalysis_phy_006_004.
- Skirris, N., Sofianos, S., Lascaratos, A., 2007. Hydrological changes in the Mediterranean Sea in relation to changes in the freshwater Budget: a numerical modelling. *J. Mar. Syst.* 65 (1–4), 400–416. <https://doi.org/10.1016/j.jmarsys.2006.01.015>.
- Smith, W.H.F., Sandwell, D.T., 1997. Global sea floor topography from satellite altimetry and ship depth soundings. *Science* 277, 1956–1962.
- Somot, S., Sevault, F., Déqué, M., 2006. Transient climate change scenario simulation of the Mediterranean Sea for the twenty-first century using a high-resolution ocean circulation model. *Clim. Dyn.* 27 (7–8), 851–879.
- Tintoré, J., Vizoso, G., Casa, B., Heslop, E., Pascual, A., Orfila, A., et al., 2013. SOCIB: the Balearic Islands coastal ocean observing and forecasting system responding to science, technology and society needs. *Mar. Technol. Soc. J.* 47 (1), 101–117.
- Troupin, C., Beltrán, J.P., Heslop, E., Torner, M., Garau, B., Allen, J., Tintoré, J., 2015. A toolbox for glider data processing and management. *Methods Oceanogr.* 13, 13–23.
- Undén, P., et al., 2002. The HIRLAM version 5.0 model. HIRLAM documentation manual (HIRLAM Scientific Documentation). Available at <http://www.knmi.nl/hirlam/SciDocDec2002.pdf> (or from Hirlam-5 Project, SMHI, S-60176, Norrköping, Sweden).
- Vargas-Yáñez, M., Moya, F., García-Martínez, M.C., Zunino, P., Tel, E., Plaza, F., Salat, J., Pascual, J., López-Jurado, J.L., Serra, M., 2010. Climate change in the Western Mediterranean Sea 1900–2008. *J. Mar. Syst.* 82, 171–176. <https://doi.org/10.1016/j.jmarsys.2010.04.013>.
- Vargas-Yáñez, M., Zunino, P., Schroeder, K., López-Jurado, J.L., Plaza, F., Serra, M., Castro, C., García-Martínez, M.C., Moya, F., Salat, J., 2012. Extreme Western Intermediate Water formation in winter 2010. *J. Mar. Syst.* 105–108, 52–59. <https://doi.org/10.1016/j.jmarsys.2012.05.010>.
- Vargas-Yáñez, M., García-Martínez, M.C., López-Jurado, J.L., Moya, F., Balbín, R., López-Jurado, J.L., Serra, M., Zunino, P., Pascual, J., Salat, J., 2017. Updating temperature and salinity mean values and trends in the western Mediterranean: the RADMED project. *Prog. Oceanogr.* 157, 27–46. <https://doi.org/10.1016/j.pcean.2017.09.004>.
- Víúdez, A., Tintoré, J., Haney, R.L., 1996. Circulation in the Alboran Sea as determined by quasi-synoptic hydrographic observations. Part I: three-dimensional structure of the two anticyclonic gyres. *J. Phys. Oceanogr.* 26 (5), 684–706.
- Víúdez, A., Pinot, J.M., Haney, R.L., 1998. On the upper circulation in the Alboran Sea. *J. Geophys. Res.* 103 (C10), 21653–21666.